Importance of the Domain−Domain Interface to the Catalytic Action of the NO Synthase Reductase Domain†

Andrew Welland, Pierre E. Garnaud, Maki Kitamura, Caroline S. Miles, and Simon Daff*

School of Chemistry, University of Edinburgh, West Mains Road, Edinburgh EH9 3JJ, U.K.

Received May 2, 2008; Revised Manuscript Received July 23, 2008

ABSTRACT: Calmodulin (CaM) activates NO synthase (NOS) by binding to a 20 amino acid interdomain hinge in the presence of Ca^{2+}, inducing electrons to be transferred from the FAD to the heme of the enzyme via a mobile FMN domain. The activation process is influenced by a number of structural features, including an autoinhibitory loop, the C-terminal tail of the enzyme, and a number of phosphorylation sites. Crystallographic and other recent experimental data imply that the regulatory elements lie within the interface between the FAD- and FMN-binding domains, restricting the movement of the two cofactors with respect to each other. Arg1229 of rat neuronal NOS is a conserved residue in the FAD domain that forms one of only two electrostatic contacts between the domains. Mutation of this residue to Glu reverses its charge and is expected to induce an interdomain repulsion, allowing the importance of the interface and domain−domain motion to be probed. The charge-reversal mutation R1229E has three dramatic effects on catalysis: (i) hydride transfer from NADPH to FAD is activated in the CaM-free enzyme, (ii) FAD to FMN electron transfer is inhibited in both forms, and (iii) electron transfer from FMN to the surrogate acceptor cytochrome *c* is activated in the CaM-free enzyme. As a result, during steady-state turnover with cytochrome *c*, calmodulin now deactivates the enzyme and causes cytochrome *c*-dependent inhibition. Evidently, domain−domain separation is large enough in the mutant to accommodate another protein between the cofactors. The effects of this single charge reversal on three distinct catalytic events illustrate how each is differentially dependent on the enzyme conformation and support a model for catalytic motion in which steps i, ii, and iii occur in the hinged open, closed, and open states, respectively. This model is also likely to apply to related enzymes such as cytochrome P450 reductase.

Nitric oxide (NO) fulfills multiple physiological roles, as a signaling agent in neurotransmission and vasodilation, and produces reactive oxygen species responsible for the destruction of pathogens by the immune system (*1, 2*). The mammalian NO synthases (NOS)[1] produce NO by the two-step oxidation of L-arginine, via *N*-hydroxyarginine, to citrulline, utilizing 2 equiv of molecular oxygen and 1.5 equiv of NADPH as substrates (*3, 4*).

Of the three NOS isoforms in mammals, endothelial NOS (eNOS) and neuronal NOS (nNOS) are expressed constitutively, with their activity being regulated by intracellular Ca^{2+} concentration, via the reversible binding of calmodulin (CaM). The third, inducible NOS (iNOS), binds CaM at low Ca^{2+} concentrations and is regulated at the transcriptional level (*4*). Each isoform is homodimeric, with subunits that comprise an N-terminal oxygenase domain linked to a C-terminal reductase domain by a CaM binding site (of approximately 20 amino acids). The reductase domain of one subunit supplies electrons to the oxygenase domain of the other subunit (*5, 6*) via a large-scale conformational movement, which is integral to the CaM-dependent activation mechanism but is largely undefined.

The oxygenase domain binds a cysteine-ligated heme, tetrahydrobiopterin (H_4B), and L-arginine, forming the unique active site where oxygen is bound and NO synthesis takes place (*7*−*9*).

The reductase domain contains FAD, FMN, and NADPH, has a structure analogous to that of NADPH−cytochrome P450 reductase (CPR) (*10, 11*), and can be divided into an N-terminal flavodoxin-like domain that binds FMN and a C-terminal FAD domain that is similar to ferrodoxin $NADP^+$ reductase (FNR) (*12*). Electrons are derived from NADPH dehydrogenation at the FAD and passed sequentially through FMN to the heme in the oxygenase domain. The FMN oscillates between the semiquinone and hydroquinone states during catalysis, serving as a simple one-electron donor (*13*), and it is this electron transfer that is both the rate-determining step in NO synthesis and the event activated by CaM (*14*).

The isolated reductase domain (nNOSrd) is also activated by the binding of CaM (*15*), with the transfer of electrons

† This work was supported in part by Wellcome Trust Grant 066774, by a University Royal Society fellowship to S.D., by a BBSRC Ph.D. studentship to A.W., and by a University of Edinburgh, School of Chemistry, Christina Millar studentship to P.E.G., who is currently at the Center for Infectious Diseases and Vaccinology, Arizona State University.

* To whom correspondence should be addressed. E-mail: Simon.Daff@ed.ac.uk. Tel: +44 (0)131 650 7378.

[1] Abbreviations: nNOSrd, recombinant neuronal nitric oxide synthase reductase domain; nNOS, rat neuronal nitric oxide synthase; CPR, mammalian cytochrome P450 reductase; CaM, calmodulin; nNOS-FMNCaM, the recombinant FMN-binding subdomain of rat nNOS with bound CaM; EGTA, ethylenebis(oxyethylenenitrilo)tetraacetic acid; DTT, dithiothreitol; PMSF, phenylmethanesulfonyl fluoride; OTTLE, optically transparent thin-layer electrode; SI, small insertion in nNOSrd; AI, autoinhibitory insert in nNOSrd; CT, C-terminal extension to nNOSrd.

10.1021/bi800787m CCC: $40.75
Published on Web 08/22/2008

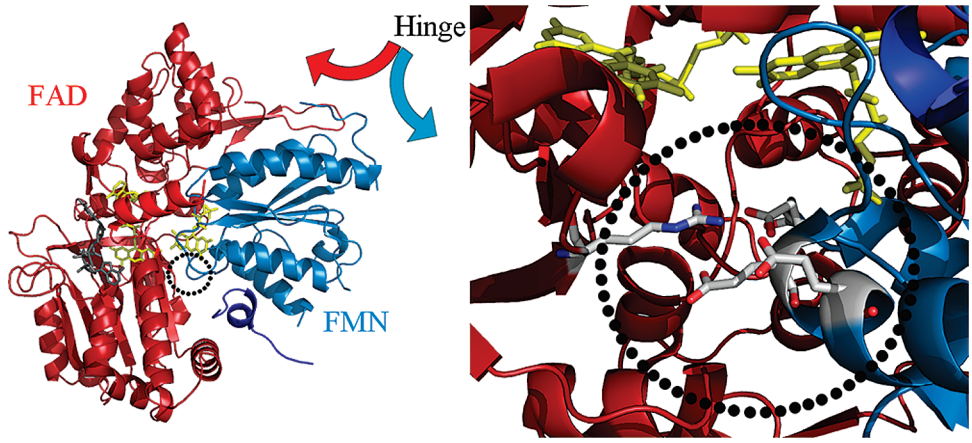

FIGURE 1: Structure of nNOSrd (PDB code 1TLL) showing the FAD-binding domain in red, the FMN-binding domain in blue, bound FAD and FMN in yellow, and NADPH in gray. Right-hand side: Close-up of the interface between the FAD- and FMN-binding domains, with residues Arg1229, Glu762, Glu816, and Glu819 in stick conformation.

to external electron acceptors such as ferricyanide or cytochrome *c* and NADPH-dependent flavin reduction all being accelerated (*16*). Given that there is little effect on the reduction potentials of the flavins (*17*), it has been proposed that a conformational rearrangement in the reductase domain induced by the binding of CaM is responsible (*18, 19*).

There are a number of unique structural features involved in suppressing electron transfer through CaM-free nNOSrd, including a 42 amino acid insert in the FMN domain (*20, 21*) and a 33 residue extension to the C-terminus (*22, 23*) that have both been shown to be autoinhibitory domains. Deletion of either of these activates electron transfer through the CaM-free reductase domain and synthesis of NO in the holoenzyme (*24*). It has recently been proposed that the concerted action of these and bound calmodulin are essential for activation (*25*). Furthermore, there is a four to seven residue insertion in the hinge region between the FMN and FAD domains (*26*) and phosphorylation sites (*27, 28*) that have roles in the protection of the CaM-binding linker and in defining the level of Ca^{2+} sensitivity of the enzyme.

The binding of NADPH is also important in the Ca^{2+}/CaM-dependent regulation of nNOSrd, through its interactions with residues Arg1400 (*29*) at the 2′-phosphate position and Phe1395 (*30, 31*), which π-stacks with the FAD isoalloxazine ring system. When NADPH binds to the CaM-free enzyme, electron transfer from the FMN to external electron acceptors is inhibited; this is thought to be caused by the reductase domain adopting a compact "locked" conformation in which the FMN is inaccessible (*32*).

In the absence of sufficient structural information, the precise mechanism by which CaM activates NO synthase is unclear. However, it appears that CaM binding induces freedom of conformational motion in the reductase domain, allowing the FMN domain to oscillate between positions in which the FMN is located close to the FAD and close to the heme (*41, 42*). The fluidity, speed, and size of this movement are unknown. The various autoinhibitory features appear to stabilize the conformation of the protein in which the FMN is close to the FAD, as shown in the crystal structure of nNOSrd (Figure 1) (*11*).

This paper addresses the relationship between conformational movement and catalytic action in the reductase domain of nNOS by alteration of the interface between the FAD and FMN domains. A close-up of the interface (Figure 1) shows the site of an interaction between Arg1229 on the FAD domain and an acidic patch on the FMN domain consisting of Glu762, Glu816, and Glu819. This is one of only two electrostatic contacts between the domains. The arginine residue is conserved in CPR (*10*) but only interacts with a solitary glutamic acid. In order to destabilize the interface in nNOSrd, we mutated Arg1229 to Glu, reversing its charge and introducing a probable electrostatic repulsion. Kinetic analysis of the mutant shows profound changes to several individual catalytic events, which are interpreted in terms of the above model.

EXPERIMENTAL PROCEDURES

Materials. All reagents were purchased from Sigma Aldrich Ltd., unless otherwise stated.

Generation of the nNOS R1229E Mutant. The R1229E mutation was generated in both full-length rat nNOS and nNOSrd using the Stratagene QuikChange XL site-directed mutagenesis kit. The templates for the reaction were the nNOS pCWori construct (*33*) and pCRNNR (*34*), respectively. The primers used were R1229EFor (5′GTCCCCTGCTTCGTGGAAGGTGCCCCTAGCTTC) and R1229ERev (5′GAAGCTAGGGGCACCTTCCACGAAGCAGGGGAC) which substitute Arg1229 with glutamic acid. Mismatches are underlined. Products containing the required mutation were selected by automated sequencing. Further sequencing confirmed that no secondary mutations were present. The resulting plasmids pCM199 and pCM226 (containing the R1229E nNOSrd and R1229E nNOS, respectively) were then transferred to *Escherichia coli* BL21(DE3) for expressing the mutant enzymes. pGroESL (*35*), which expresses chaperone proteins, was cotransformed into the *E. coli* strain with the full-length nNOS mutant.

Preparation of Wild-Type and R1229E nNOSrd, R1229E nNOS, and Calmodulin. Purification of wild-type and mutant nNOSrd was carried out using 2′,5-ADP−agarose (1 × 20 cm) and CaM−agarose (1 × 10 cm), as previously described (*32*) with the additional use of protease inhibitor cocktail at the cell lysis stage. In order to keep the bound FMN in the semiquinone form, all buffers were degassed with nitrogen prior to use. Enzyme concentration was calculated using an extinction coefficient of 20940 M^{-1} cm^{-1} (*36*). CaM was purified using the established protocol (*32*).

R1229E nNOS was purified using 50 mM Tris-HCl, pH 7.5, 0.1 M KCl, 10% glycerol, and 1 mM DTT (buffer A), with the addition of 3 EDTA-free protease inhibitor tablets, 1 mM PMSF, and 4 mM H_4B before sonication on ice. The lysate was centrifuged at 48500*g* for 1 h and the supernatant passed through a DEAE column (2 × 5 cm) and eluted with buffer A. $CaCl_2$ was added to 5 mM followed by loading onto a CaM−agarose (1 × 10 cm) column before washing with buffer A plus 1 mM $CaCl_2$ and elution with buffer A plus 5 mM EGTA. Wild-type nNOS was generated in the same manner.

The isolated FMN domain of rat nNOS (nNOSFMNCaM) was coexpressed and copurified with bound calmodulin using anion-exchange chromatography as described previously (*36*). This mutant consists of residues 695−946 and was always handled in the presence of 1 mM Ca^{2+} to ensure bound CaM and to maintain stability. Reduced nNOSFMN-CaM was prepared in an anaerobic chamber by reduction using sodium dithionite followed by G25 gel filtration chromatography.

Steady-State Turnover. The activity of nNOSrd was characterized by the reduction of electron acceptors cytochrome *c* (from horse heart) and potassium ferricyanide (FSA Laboratory supplies) using a Cary 50 UV/vis or Shimadzu UV-1601 spectrophotometer. Assays were carried out at 25 °C as described previously (*21*) and initiated by the addition of enzyme (10−40 nM), NADPH (1 mM), and either EGTA (1 mM) or Ca^{2+}/CaM (1 mM/100 μM). All experiments were performed in 50 mM Tris-HCl, pH 7.5, and 0.1 M NaCl. Extinction coefficients used were 21 mM^{-1} cm^{-1} for the difference in molar absorbance for reduced and oxidized cytochrome *c* at 550 nm, 1.01 mM^{-1} cm^{-1} for oxidized ferricyanide at 401 nm, and 6.22 mM^{-1} cm^{-1} for NADPH at 340 nm.

Flavin Reduction Kinetics. Pre-steady-state reduction of the bound flavins of nNOSrd was carried out by stopped-flow (Applied Photophysics) mixing of 10 μM enzyme with 100 μM NADPH, in the presence or absence of Ca^{2+}/CaM. The change in absorbance at 457nm was monitored, and the resultant traces were fitted using Origin 7.0 (Microcal). Full spectra were recorded using a diode-array detector, at 2.5 ms intervals. The enzyme was either one-electron reduced by titration against dithionite in an anaerobic glovebox (Belle Technology) or fully oxidized by addition of excess potassium ferricyanide followed by size exclusion chromatography (Sephadex G-25).

In the case of inhibition studies, 30 μM ferrous cytochrome *c* was added to the enzyme before mixing. This was prepared by titration with sodium dithionite and removal of excess reductant by size exclusion chromatography (Sephadex G-25).

Cytochrome c Reduction. Stopped-flow cytochrome *c* reduction experiments were carried out as previously reported (*32*). Cytochrome *c* (4 μM) was mixed with 10 μM sodium dithionite-reduced nNOSrd in the presence and absence of CaM and the presence and absence of NADPH. Substrate (cytochrome *c*) inhibition studies were also conducted in the presence of 30 μM ferrous cytochrome *c*. Reduction was observed at 550 nm, and pseudo-first-order rate constants were calculated by fitting the resultant traces to single-exponential functions. Second-order rate constants were determined by dividing the pseudo-first-order constants by the enzyme concentration. The second-order behavior of this reaction was confirmed for R1229E nNOSrd by varying the concentration of enzyme in the reaction from 7 to 15 μM. The rate constant increased linearly with concentration and had a second-order constant of 39 mM^{-1} s^{-1} as for the wild-type enzyme (*32*).

Spectroelectrochemistry. Spectroelectrochemical analysis of nNOSrd was carried out using approximately 0.2 mM enzyme in an OTTTLE cell of 0.2 mm path length as previously described (*36*), with the addition of the mediators FMN (15 μM), benzyl viologen (20 μM), methyl viologen (30 μM), 2-hydroxy-1,4-naphthoquinone (30 μM), and 5-hydroxy-1,4-naphthoquinone (30 μM). The Ag/AgCl reference electrode was calibrated against indigotrisulfonic acid and FMN and found to be +205 ± 2 mV relative to the standard hydrogen electrode (SHE). All electrode potentials were corrected accordingly.

UV−visible spectra were collected at 30 mV intervals in the reductive and oxidative directions, and the absorbance at 456 and 540 nm was plotted vs applied potential. Both sets of data were fitted simultaneously to a double Nernst-type equation (eq 3) using Origin 7.5 (Microcal). The equation has three parameters: *a*, *b*, and *c* representing the absorption coefficients of the flavin oxidized, semiquinone, and reduced states, respectively. These are allowed to vary at each different wavelength, whereas the four reduction potential values are the same at both wavelengths. The FMN and FAD are assumed to have the same extinction coefficients in their respective redox states, which is a good approximation for the wavelengths used according to parameters derived from the single domains (*36*). No additional constraints were imposed on the fitting process, and convergence was achieved from any reasonable estimate of the parameters prior to fitting. $R^2 = 0.99692$ and 0.99748 for the wild-type and R1229E data, respectively.

NO Synthesis. Full-length nNOS was assayed for NOS activity by monitoring the conversion of oxyhemoglobin to methemoglobin at 401 nm, using an extinction coefficient of 49000 M^{-1} cm^{-1}. The reaction was started when nNOS (~20 nM) was added to a cuvette containing 10 μM oxyhemoglobin, 100 μM NADPH, 10 units/mL superoxide dismutase (SoD) and catalase, 10 μM H_4B, 0.1 mM DTT, 1 mM L-Arg, 50 μg/mL CaM, and 1 mM $CaCl_2$ and made up to 1 mL with Tris-HCl (50 mM, pH 7.5) buffer. NADPH oxidation rates were also collected by monitoring at 340 nm in the absence of oxyhemoglobin, extinction coefficient 6220 M^{-1} cm^{-1}.

RESULTS

Steady-State Turnover. Cytochrome *c* reduction by nNOS is activated by CaM binding; this effect has been shown to be reproduced in nNOSrd. Rate constants for the steady-state reduction of cytochrome *c* by wild-type nNOSrd are plotted in Figure 2A and fitted to the Michaelis−Menten equation. The kinetic parameters are given in Table 1. The k_{cat} for cytochrome *c* reduction is enhanced 10-fold upon binding of CaM, as shown previously (*16*). Figure 2B plots the data obtained from the steady-state reduction of cytochrome *c* by R1229E nNOSrd. In the CaM-free assay, the rate initially increases with the concentration of cytochrome *c*, to a maximum of 7.5 s^{-1}; however, it then decreases at

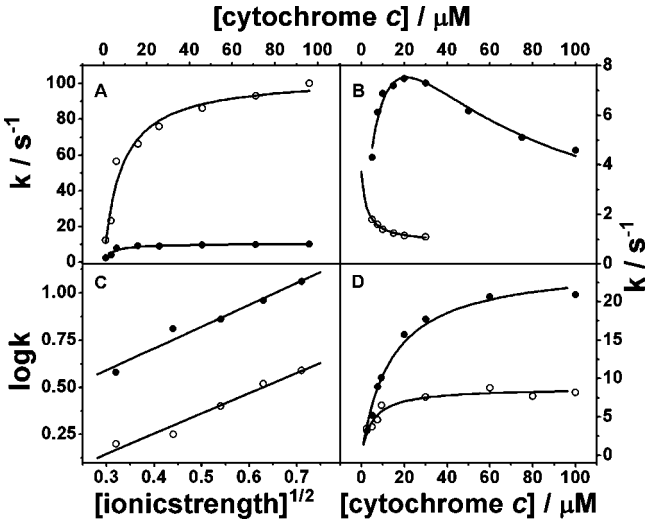

FIGURE 2: Steady-state cytochrome *c* reduction. (A) Wild-type data fitted to the Michaelis−Menten equation. (B) R1229E under standard assay conditions, with CaM-free data fitted to eq 1 and CaM-bound data fitted to eq 2. (C) R1229E assayed with 15 μM cytochrome *c* and increasing concentrations of NaCl. The linear relationship, fitted according to Debye−Huckel theory, has a gradient of 1 in both cases. (D) R1229E assayed in 1 M NaCl buffer and shown fitted to the Michaelis−Menten equation. All plots show assays performed in the absence (closed circles) and presence (open circles) of CaM at 25 °C, as described in Experimental Procedures. All derived parameters are listed in Table 1.

Table 1: Steady-State Turnover of Cytochrome *c*[a]

enzyme	CaM	k_{cat} (s^{-1})	K_m (μM)	K_i (μM)
wild type	−	10.4 ± 0.4	3 ± 1	
	+	104 ± 6	8 ± 2	
wild type + high salt buffer	−	23 ± 1	12 ± 2	
	+	95 ± 6	12 ± 3	
R1229E	−	14.8 ± 1.8	10 ± 2	44 ± 9
	+	3.4 ± 1.8[b]		2 ± 2
R1229E + high salt buffer	−	24.3 ± 1.4	14 ± 2	
	+	8.8 ± 0.5	5 ± 1	

[a] The rate of cytochrome *c* reduction was measured at 25 °C as detailed in Experimental Procedures and plotted in Figure 2. [b] Should be considered a lower estimate, given that the K_m could not be obtained.

concentrations greater than 20 μM. This indicates that excess cytochrome *c* is inhibiting catalytic turnover. When CaM is present, the rate of cytochrome *c* reduction is much lower (<2 s^{-1}), and inhibition is apparent at cytochrome *c* concentrations as low as 2 μM. The CaM-free data fit well to a model for substrate inhibition in which the substrate (cytochrome *c*) binds to an unproductive form of the enzyme (eq 1). Inhibition occurs with the CaM-bound mutant even at low concentrations of cytochrome *c*, so these data are fitted to a simpler inhibition equation (eq 2). The difficulty in obtaining accurate rate constants at low concentrations of cytochrome *c* compromises the accuracy of these data. It is also impossible to obtain a K_m value. The value for k_{min} is the estimated rate constant for steady-state turnover at high cytochrome *c* concentration (0.9 s^{-1}), and k_{max} is the rate constant estimated with no inhibition (i.e., the *y*-axis intercept). Note that the latter value is likely to be underestimated by the fact that decreasing cytochrome *c* concentrations will cause the observed turnover rate to decrease as the K_m is approached. However, it is clear that the rate of reduction is markedly slower for R1229E nNOSrd when CaM is bound, an occurrence not seen in other reductase domain mutants, although this is likely to be influenced by

Scheme 1: Sequential Reduction of Fully Oxidized and One-Electron Reduced Forms of nNOSrd by Excess NADPH

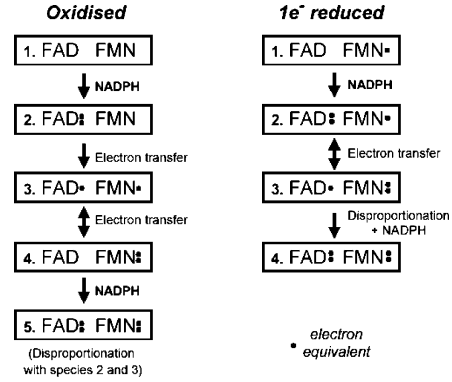

the inhibition effect. The overall effect of the mutation on the observed rate of cytochrome *c* reduction by the CaM-bound enzyme is particularly large: a decrease from 100 s^{-1} to around 2 s^{-1}. The mutation therefore appears to induce two separate effects. It decreases the rate of electron transfer through the CaM-bound enzyme and introduces substrate inhibition at high cytochrome *c* concentrations. Both of these may be due to changes in the electrostatic interactions within the domain interface.

The dependence of the rate constant for steady-state turnover on substrate concentration (*S*) with substrate inhibition (K_i) is given by eq 1.

$$\frac{k_{cat}[S]}{[S]\left(1+\frac{[S]}{K_i}\right)+K_m} \quad (1)$$

The dependence of the rate constant for steady-state turnover on substrate concentration (*S*) with partial substrate inhibition (K_i) for $S \gg K_m$ is given by eq 2.

$$\frac{k_{max}K_i + k_{min}[S]}{K_i + [S]} \quad (2)$$

In order to test this theory, the assay was repeated at varying levels of ionic strength, i.e., increased NaCl concentration in the assay buffer. Figure 2C shows a linear dependence of the log of the rate constant for cytochrome *c* reduction at 15 μM versus the square root of ionic strength. According to Debye−Huckel theory, the primary kinetic salt effect obtained from the gradient of the plot gives the ionic charge interaction involved. For both the CaM-free and CaM-bound mutant there is a net unit charge interaction of 1. It seems likely therefore that the high salt concentrations can compensate for the negative−negative repulsion across the domain−domain interface caused by the mutated residue and increase the rate of interflavin electron transfer. As expected, the electrostatic component of the interaction is unaltered by the binding of CaM.

When the salt concentration was increased to 1 M (Figure 2D), the steady-state kinetic data for R1229E nNOSrd fitted to the Michaelis−Menten equation, giving catalytic turnover rates of 25 s^{-1} (CaM-free) and 9 s^{-1} (CaM-bound). It is interesting to note that the activity of the enzyme is still decreased by more than 2-fold upon binding of CaM, which is opposite to the effect seen in the wild-type enzyme.

Flavin Reduction Kinetics. The first step in the turnover of nNOSrd is hydride transfer from NADPH to bound FAD

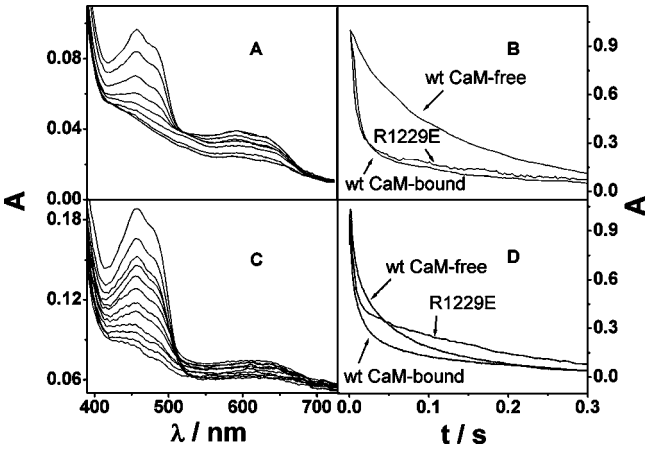

FIGURE 3: Pre-steady-state reduction of nNOSrd by NADPH. (A) UV−visible spectra of reaction with one-electron reduced R1229E nNOSrd. (B) Kinetic traces at 457 nm for one-electron reduced CaM-free and bound wild-type nNOSrd and the R1229E mutant. (C) UV−visible spectra of reaction with fully oxidized R1229E nNOSrd. (D) Kinetic traces at 457 nm for fully oxidized CaM-free and bound wild-type nNOSrd and the R1229E mutant. Enzyme samples were approximately 6 μM and NADPH was 100 μM after mixing. All traces were fitted to a double-exponential equation over 1 s. The kinetic parameters are listed in Table 2.

Table 2: Rate Constants for Pre-Steady-State Flavin Reduction by Excess NADPH[a]

enzyme	Ca^{2+}/CaM	k_1 [Abs (%)]	k_2 [Abs (%)]
wild type−FMN semiquinone	−	35 ± 1 (20)	6.5 ± 0.1 (80)
	+	93 ± 2 (80)	5.1 ± 0.1 (20)
R1229E−FMN semiquinone	−	138 ± 3 (73)	5.6 ± 0.1 (27)
	+	162 ± 4 (80)	4.3 ± 0.1 (20)
wild type−FMN oxidized	−	65 ± 2 (40)	5.9 ± 0.1 (60)
	+	73 ± 2 (79)	3.6 ± 0.1 (21)
R1229E−FMN oxidized	−	169 ± 5 (52)	4.0 ± 0.1 (48)
	+	156 ± 6 (57)	5.6 ± 0.1 (43)

[a] The rate of flavin reduction was measured at 25 °C as detailed in Experimental Procedures and plotted in Figure 3. Abs values indicate the proportion of the total absorbance change occurring in each kinetic phase.

and can be investigated by the stopped-flow mixing of nNOSrd with an excess of NADPH (*32*). In these experiments, the enzyme may react further depending on the oxidation state of the FMN; if oxidized, the bound FMN can accept two electrons from FAD and allow the FAD to react with a second molecule of NADPH (Scheme 1). During catalysis, however, the FMN is bound as an air-stable semiquinone. This form of nNOSrd reacts with NADPH to cause the enzyme to be three-electron reduced (Scheme 1). Note that electron transfer from FAD to FMN in this state causes little change to the visible spectrum. In order for further reduction of the flavins to occur, intermolecular electron transfer must occur between different enzyme molecules; this is known to occur through disproportionation, probably via the more accessible FMN cofactor (*32, 36*).

Data for the reduction of one-electron reduced nNOSrd are shown in Figure 3A,B. The kinetic traces at 457 nm were fitted to double-exponential fitting functions and the derived parameters listed in Table 2. CaM-free wild-type nNOSrd is reduced by NADPH in a biphasic process with a large slow phase of rate constant 6.5 s^{-1}. The reduction process observed is undoubtedly hydride transfer from NADPH to FAD; however, it is unclear why this is biphasic. The results are consistent across numerous enzyme samples, and it is likely that heterogeneity within the sample causes some molecules to react faster than others. CaM-bound wild-type nNOSrd is rapidly reduced by hydride transfer from NADPH at around 100 s^{-1}. This is then followed by further slow reduction initiated by intermolecular electron transfer and disproportionation of flavin semiquinones; this contributes approximately 20% of the absorbance change at 457 nm. R1229E nNOSrd exhibits no significant dependence on the presence of CaM. As with the CaM-bound wild-type enzyme, hydride transfer from NADPH to FAD occurs rapidly and is followed by a slow disproportionation phase of similar magnitude. The disproportionation phase can also be observed from the decrease in absorbance at 600 nm (Figure 3A) (*32*).

It appears that the rate of reduction of FAD by NADPH is faster in CaM-bound nNOSrd than CaM-free and that the R1229E mutant is reduced at least as quickly as the CaM-bound enzyme, regardless of whether CaM is present or not. The mutation therefore appears to increase the rate of FAD reduction by NADPH in the CaM-free enzyme.

Reduction of fully oxidized nNOSrd is complicated by the reaction of the enzyme sequentially with 2 equiv of NADPH. Thus hydride transfer from NADPH to FAD is followed by two electron transfers from FAD to FMN before the FAD can react with a second molecule of NADPH (Scheme 1). Kinetic data for the reduction of fully oxidized WT nNOSrd and the R1229E mutant are included in Figure 3C,D. As before, the kinetic traces at 457 nm were fitted to double-exponential fitting functions and the derived parameters listed in Table 2. From Figure 3D it is clear that once again CaM-bound wild-type nNOSrd is reduced more quickly than CaM-free. However, the rate constants shown in Table 2 indicate that there is a shift in amplitude for the fast phase from 40% to 79% on the addition of CaM rather than an increase in the rate constant. As with the one-electron reduced enzyme, this indicates that some molecules in the CaM-free sample react faster with NADPH than others. Previous analyses of similar data have failed to reach a satisfactory explanation for the different phases in this reaction (*18, 31, 32, 43, 44*), and further studies are necessary to explain the full effect of CaM binding on the NO synthase reductase domain.

For the R1229E mutant, the data are very different and easier to interpret. The kinetic trace in Figure 3D shows a very rapid first phase, followed by a very slow second phase; a pronounced phase-change is apparent. Both phases contribute 50% of the absorbance change (Table 2), indicating that half of the flavins in the sample are reduced in each phase. In order to gain further insight, the absorbance changes at 592 nm should also be considered (Figure 4), which report on the formation and loss of flavin semiquinone species during the reduction process. For the CaM-free wild-type enzyme, a rapid increase in semiquinone content is observed, followed by a decrease (Figure 4A). This is consistent with the transfer of one electron from FAD to FMN (causing the increase) followed by the transfer of a second electron (causing the decrease) as in Scheme 1. For the CaM-bound enzyme the two transfers are faster (Figure 4B), leading to a very transient accumulation of semiquinone. The slow increase observed over 4 s is caused by disproportionation of flavins to thermodynamic equilibrium. For the R1229E

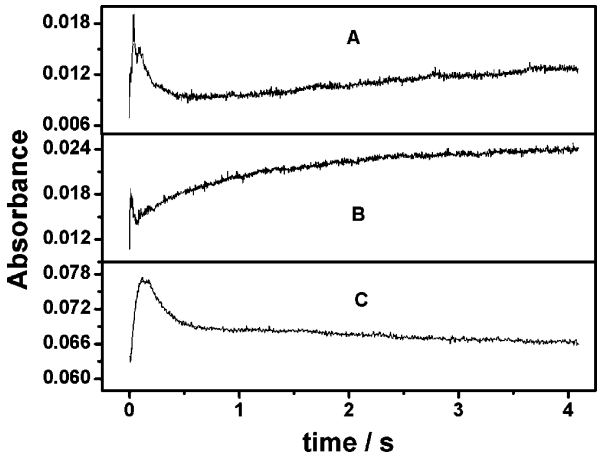

FIGURE 4: Pre-steady-state reduction of fully oxidized nNOSrd by NADPH. Time-dependent traces for the absorbance associated with the FMN semiquinone at 592 nm: (A) wild-type CaM-free, (B) wild-type CaM-bound, and (C) R1229E CaM-free. Traces are derived from the same experiments as in Figure 3D.

mutant, the initial buildup of semiquinone is much slower than for either CaM-free or CaM-bound wild-type enzyme (Figure 4C), as is the subsequent decay at 592 nm. A larger amount of semiquinone also accumulates. The 592 nm data are shown fitted to a kinetic model for two sequential steps, both with rate constants of 10 ± 5 s^{-1}, i.e., much slower than the rate of NADPH to FAD hydride transfer but corresponding to the rate of the second phase of reduction at 457 nm (approximately 5 s^{-1} for the two-electron transfer). The electron transfers from FAD to FMN appear therefore to have been dramatically slowed by the mutation, particularly with respect to the CaM-bound wild-type enzyme. It is now clear that the two phases observed in the reduction trace at 457 nm for the R1229E mutant represent the sequential reduction of the FAD and FMN cofactors by 2 equiv of NADPH. For the one-electron reduced mutant enzyme, NADPH to FAD hydride transfer has been shown to occur rapidly and completely, whereas for the oxidized enzyme, interflavin electron transfer slows down the reaction with the second equivalent of NADPH and is rate-limiting for this step.

All flavin reduction experiments with the R1229E mutant were repeated in the presence of ferrous cytochrome *c*, but the hydride transfer step did not appear to be affected (data not shown).

Cytochrome c Reduction. The transfer of an electron from hydroquinone FMN to cytochrome *c* is the final step in the turnover of nNOSrd and provides an estimate of the accessibility of the bound FMN. It can be measured by the stopped-flow mixing of chemically reduced enzyme with a substoichiometric amount of cytochrome *c*, in the presence and absence of calmodulin and NADPH. This experiment has previously been used to reveal that the CaM-free NADPH-bound wild-type enzyme is in a locked FMN-inaccessible conformation, where the binding of NADPH causes the second-order rate constant to drop from 15 μM^{-1} s^{-1} to 1 μM^{-1} s^{-1}, while the binding of CaM enhances it to >35 μM^{-1} s^{-1}, releasing the lock and allowing the rapid transfer of an electron from FMN to cytochrome *c* (*32*).

Figure 5 compares traces for pre-steady-state cytochrome *c* reduction by wild-type nNOSrd with and without bound CaM, the R1229E mutant, and the isolated nNOS FMN

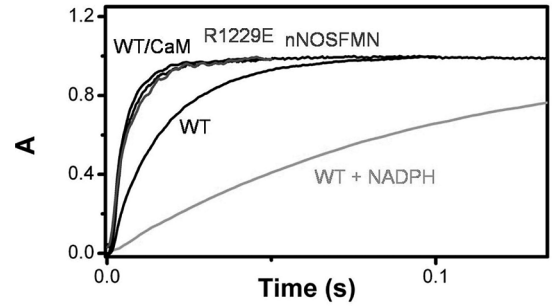

FIGURE 5: Pre-steady-state reduction of cytochrome *c* by reduced nNOSrd. Normalized kinetic traces showing the second-order reduction of cytochrome *c* (~4 μM) by wild-type and R1229E nNOSrd and the CaM-bound nNOS FMN domain. All enzyme concentrations were 10 μM after mixing.

domain under the same conditions. For R1229E nNOSrd in the presence or absence of NADPH and CaM, the second-order rate constant was 39 μM^{-1} s^{-1}, showing that the bound FMN is always accessible to cytochrome *c*. The presence of NADPH and absence of CaM is unable to induce a locked conformation in the mutant, consistent with the theory that the mutation has destabilized the domain−domain interface. Both CaM-bound wild-type and the R1229E mutant appear to have similar FMN accessibility to the isolated FMN domain, indicating that in both cases the FMN is fully exposed.

Addition of an excess of ferrous cytochrome *c* to the enzyme had no effect on the ability of the ferric cytochrome *c* to access the bound FMN (data not shown).

Spectroelectrochemistry. Potentiometric studies of nNOSrd have previously shown that the FAD is reduced in two one-electron steps of similar potential (approximately −300 mV) and that the FMN is reduced in two one-electron steps with very different potentials (approximately −300 mV and −100 mV) (*17, 36*). The FMN semiquinone is thermodynamically stabilized toward oxidation (Table 3). It also has considerable kinetic stability enabling the FMN to retain the semiquinone oxidation state during purification. Similar reduction potentials are observed in the presence and absence of CaM and even in the isolated FAD and FMN domains. The exception to this is that the FMN semiquinone loses some thermodynamic stability in the isolated domain and shifts to a lower potential. Given that the FMN does not cycle through the semiquinone-oxidized redox couple during catalysis, this is not functionally important. However, it does indicate that the presence of the FAD domain does affect the properties of the FMN.

R1229E nNOSrd was analyzed under the same conditions using OTTLE potentiometry. Figure 6A shows the UV−visible spectra produced by the stepwise reduction of the mutant by increments of 30 mV. The resultant plot of the absorbance at both 457 and 540 nm versus the applied potential (Figure 6B) was fitted using eq 3, simultaneously fitting both sets of data and yielding the midpoint reduction potentials given in Table 3. From these, it can be seen that the only potential affected by the mutation is the oxidized/semiquinone couple of FMN. The semiquinone form appears to have been thermodynamically destabilized relative to the wild-type reductase domain by approximately 30 mV. It is interesting that a point mutation in the FAD domain affects only the FMN. This is an indication that the interaction

Table 3: Midpoint Reduction Potentials of nNOSrd[a]

enzyme	FMN ox/sq	FMN sq/hq	FAD ox/sq	FAD sq/hq
wild type (−CaM)	−105 ± 6	−274 ± 7	−283 ± 8	−310 ± 7
R1229E (−CaM)	−136 ± 6	−279 ± 9	−281 ± 9	−306 ± 9
isolated domains[b]	−179 ± 3	−314 ± 3	−291 ± 3	−326 ± 3

[a] Wild type and R1229E nNOSrd were analyzed using OTTLE potentiometry as detailed in Experimental Procedures and plotted in Figures 6 and 7. Values for the absorbance parameters were as follows. For WT nNOSrd: $a_{456} = 0.055$; $b_{456} = 0.029$; $c_{456} = 0.009$; $a_{540} = 0.024$; $b_{540} = 0.073$; $c_{540} = 0.019$. For the R1229E mutant: $a_{456} = 0.037$; $b_{456} = 0.021$; $c_{456} = 0.002$; $a_{540} = 0.007$; $b_{540} = 0.043$; $c_{540} = 0.013$. [b] See ref *36*.

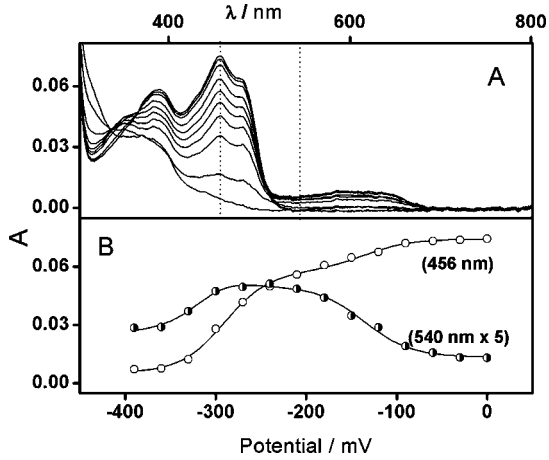

FIGURE 6: Potentiometric titration of R1229E nNOSrd. (A) UV−visible spectra collected during OTTLE titration of R1229E nNOSrd in the absence of CaM. (B) Absorbance at 456 nm (circles) and 540 nm (half-closed circles, × 5) plotted against applied potential. The data were fitted simultaneously to eq 3, yielding the midpoint reduction potentials listed in Table 3.

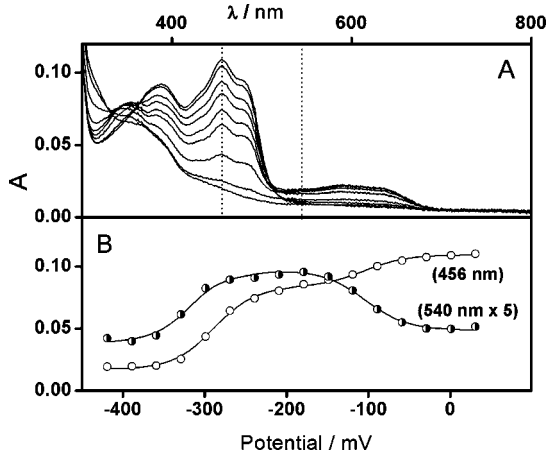

FIGURE 7: Potentiometric titration of WT nNOSrd. (A) UV−visible spectra collected during OTTLE titration of nNOSrd in the absence of CaM. (B) Absorbance at 456 nm (circles) and 540 nm (half-closed circles, × 5) plotted against applied potential. The data were fitted simultaneously to eq 3, yielding the midpoint reduction potentials listed in Table 3.

between the two subdomains is important for the stability of the semiquinone form of bound FMN and is consistent with the effect observed in the isolated FMN domain of a 74 mV shift relative to nNOSrd.

The potentiometric titration of CaM-free wild-type nNOSrd was also repeated using the OTTLE method (Figure 7). Previously, this was conducted by chemical reduction (*17*). The results are very similar to those reported earlier, although equilibration of this enzyme was particularly slow, requiring 2 h for each potential step. No evidence for CaM-dependent nNOSrd reduction potentials as reported recently (*37*) could be found.

Table 4: CaM Dependence of Steady-State Cytochrome *c* Reduction by nNOSrd and Mutants

	k_{cat} (CaM-free)/k_{cat} (CaM-bound) (%)
wild type	10
SI deletion[b]	25
AI deletion[c]	40
R1400E[d]	70
F1395S[e]	85
R1229E	435[a]
R1229E + 1 M KCl	275
CT deletion[f]	130

[a] The k_{cat} value + CaM is affected by cyt *c* inhibition, and this value is therefore an overestimate. [b] See ref *26*. [c] See ref *21*. [d] See ref *29*. [e] See ref *31*. [f] See ref *22*.

The modified Nernst equation for a system consisting of two independent redox centers with two one-electron transitions with midpoint potentials E_1, E_2 and E_3, E_4, respectively, is given by eq 3. Spectral absorption coefficients are given by *a*, *b*, and *c* for the oxidized, one-electron reduced, and two-electron reduced redox centers, respectively.

$$\frac{a\log^{-1}\left(\frac{E-E_1}{59}\right)+b+c\log^{-1}\left(\frac{E_2-E}{59}\right)}{1+\log^{-1}\left(\frac{E-E_1}{59}\right)+\log^{-1}\left(\frac{E_2-E}{59}\right)}+\frac{a\log^{-1}\left(\frac{E-E_3}{59}\right)+b+c\log^{-1}\left(\frac{E_4-E}{59}\right)}{1+\log^{-1}\left(\frac{E-E_3}{59}\right)+\log^{-1}\left(\frac{E_4-E}{59}\right)} \quad (3)$$

NO Synthesis. Full-length nNOS, both wild type and R1229E mutant, were assayed for NOS activity. There was no CaM-free activity observed for R1229E nNOS, and the CaM-bound activity was approximately 5-fold lower than for the wild-type enzyme. NADPH consumption was decreased by approximately 2.5-fold. Electron flow through the mutant has been destabilized by the mutation, probably resulting in slower flavin to heme electron transfer. Similar studies have been reported for mutations at the same interface in full-length nNOS (*38*).

DISCUSSION

Calmodulin (CaM) regulates nNOS by inducing electron transfer through to the heme of the enzyme. The mechanism of activation is centered on the reductase domain, which undergoes a structural rearrangement on binding CaM, the nature of which is uncertain. In the presence of calcium (*3, 4*), CaM binds to a flexible loop of protein connecting the oxygenase and reductase domains together. Although the structure of the holoenzyme is not known, it is likely that a large-scale motion of the FMN-binding domain is required to induce electron transfer to the heme (*18, 19*).

A number of unusual protein inserts not found in the related enzyme, cytochrome P450 reductase, are known to influence the activation process; these include an autoinhibitory loop (*20, 21*), a C-terminal extension (*22, 23*), a small insertion (*26*), and residues that are targeted for kinase-dependent phosphorylation (*27, 28*). Alteration of any of

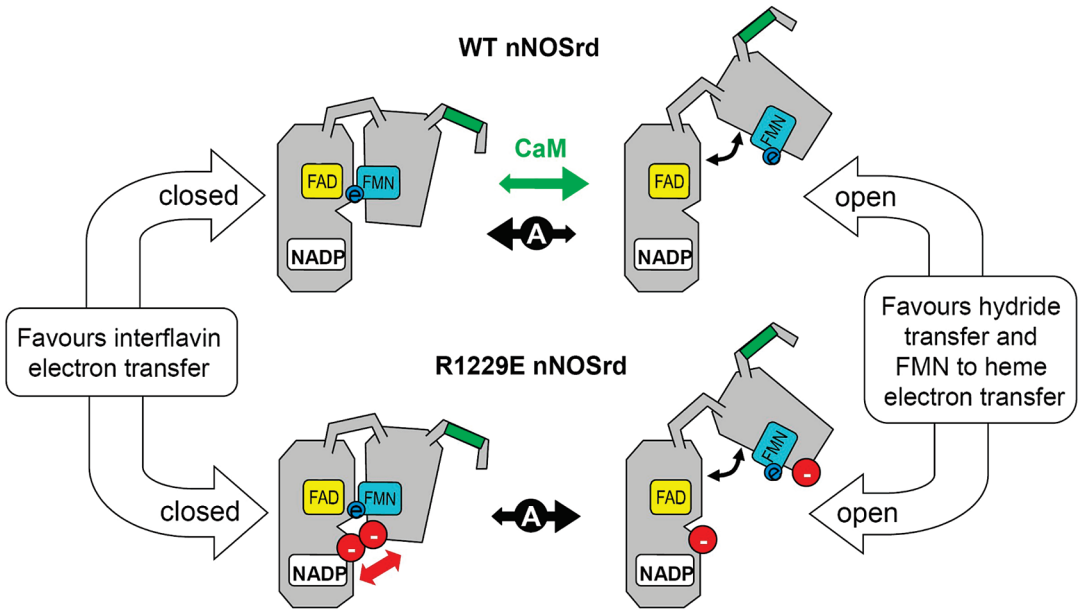

FIGURE 8: Cartoon showing how the "hinged open" and "closed" conformations of nNOSrd are influenced by CaM binding and the R1229E mutation.

these regulatory features activates electron transfer through the CaM-free reductase domain, as measured by the reduction of cytochrome *c*, but not necessarily to the NOS oxygenase domain. Table 4 summarizes previous data on the activation of steady-state cytochrome *c* reduction by CaM in NOS mutants. The mutations do not generally deactivate turnover in the presence of CaM, indicating that the NOS reductase domain is catalytically repressed in the absence of CaM, although deletion of the C-terminal extension produces an enzyme that turns over slightly faster in the presence of CaM (*22*). This and mutation of Phe1395 (*31*), which facilitates the reaction between NADPH and FAD, both also activate NO synthesis in the CaM-free state. The effect of the R1229E mutation on steady-state cytochrome *c* reduction by nNOSrd is particularly severe. In the presence of CaM, the enzyme is 30-fold slower than the wild type and 4-fold slower than in the absence of CaM. This unique shift in behavior is particularly striking given that only a single charge reversal mutation is involved and appears to be caused by two factors, disruption of FAD to FMN electron transfer and inhibition of this by the electron acceptor cytochrome *c*.

Arg1229 can be seen in the structure of nNOSrd (*11*) and in Figure 1 to interact with a patch of acidic residues on the surface of the FMN domain. Both points of contact are close to the cofactors FMN and FAD (approximately 7 Å) and are likely to be a major factor in holding the cofactors so close together (the FMN and FAD ring systems are separated by only 6 Å). The contact is conserved in cytochrome P450 reductase (*12*), suggesting that it functions to orient the two domains effectively for interflavin electron transfer.

It is apparent from the crystal structure of nNOSrd (*11*) that the autoinhibitory elements involved in repression of the enzyme lie at the interface between the FAD- and FMN-binding domains. It has been speculated that they stabilize a conformation of the CaM-free enzyme in which the FMN is "locked" into a solvent-inaccessible position (*25, 29*). This form is also stabilized by the binding of NADPH and is thought to be represented in the crystal structure (*11, 32*). All of the mutations listed in Table 4 have multiple effects on the CaM-free enzyme, often characterized by increased cytochrome *c* reductase activity, faster rates of flavin reduction, and decreased response to CaM. It is likely that destabilization of the FAD−FMN domain interface is a common cause of these effects. Arg1229 is not part of an autoinhibitory feature or of any other catalytic unit. Therefore, its mutation reports directly on the importance of the interface to the different steps of catalysis.

The catalytic action of nNOSrd involves three primary events: hydride transfer to FAD, electron transfer from FAD to FMN, and electron transfer from FMN to heme or surrogate electron acceptor. Each has been proposed to be activated by CaM (*14, 16, 18, 32*). Given the putative role of the autoinhibitory inserts in stabilizing the domain−domain interface, and of CaM in counteracting the effect, it seems likely that CaM may affect all three of the steps simultaneously. If the multiple effects of CaM result from destabilization of the interface, then the R1229E mutation should induce similar properties. This is the case for hydride transfer from NADPH to FAD and electron transfer to cytochrome *c*; however, the mutation does not activate NO synthesis, which appears to require an additional CaM-dependent structural change not involving the interface directly. The effect on FAD to FMN electron transfer is, on the other hand, more dramatic in the mutant, with little observed effect in the wild-type enzyme on CaM binding.

Hydride Transfer. The first chemical step of NO synthesis is the transfer of a hydride from NADPH to FAD. This is most easily monitored by stopped-flow reaction of enzyme with an excess of NADPH. The decrease in the main peak at 456 nm (Figure 3) reports primarily on flavin reduction originating from hydride transfer to the FAD. As the data in Figure 3B confirm, CaM increases the rate of hydride transfer in fully oxidized wild-type nNOSrd, although the actual rate constants determined from fitting the data show a shift in the amplitudes from the slow to the fast kinetic phases rather than a large change in the rate constants (Table 2). Note also that two consecutive reactions with NADPH occur with this enzyme form. For the R1229E mutant the results are

more obvious; with two exponentials of equal amplitude, it is clear that the first hydride transfer is fast and the second is slow. The reason for this is a slow interflavin electron transfer step occurring between the two hydride transfers. Note that it is apparent from Figure 3B that removing CaM from nNOSrd and introducing the R1229E mutation clearly influence different steps of the reduction process.

Further insight is gained from considering hydride transfer to the one-electron reduced enzyme by NADPH. This is the natural reaction of the enzyme and should only report on a single hydride transfer, with subsequent disproportionation of the flavin semiquinones occurring in a slow phase. For the wild-type enzyme, hydride transfer is generally slow (6.5 s^{-1} for the large phase) in the absence of CaM and fast (93 s^{-1}) with CaM bound. Presumably the R1229E mutant favors a "hinged open" conformation in which hydride transfer is rapid and interflavin electron transfer is slowed. It is logical to consider that the converse is also true, i.e., that hydride transfer in the "hinged closed" or "locked" conformation is slowed and interflavin electron transfer is rapid. (The two flavin rings are only 6 Å apart in the hinged closed state presented in the crystal structure, and the NADP is bound in an unproductive conformation.) This point is worthy of further investigation in the wild-type enzyme and may be fundamental to the mechanism of CaM-dependent enzyme activation. If the stability of the domain−domain interface determines the rate of hydride transfer from NADPH to FAD by controlling the rate at which the enzyme can hinge open (approximately 6.5 s^{-1} CaM-free), then the rate of electron transfer from FAD to FMN in the R1229E mutant conversely depends on the rate at which the enzyme can hinge closed (approximately 10 s^{-1}), if it can access this state at all. The values in Table 2 indicate that the rate constants for both hydride and interflavin electron transfer increase by at least an order of magnitude when the appropriate conformation is stabilized.

Interflavin Electron Transfer. The fact that cytochrome *c* is able to inhibit interflavin electron transfer in the mutant enzyme suggests that the FAD and FMN domains separate enough to allow another protein to access the interface. This indicates that the FMN domain is able to move a large distance during catalysis, which may be a feature of electron transfer to the NOS heme in the holoenzyme. In fact, the short-range nature of electrostatic interactions such as the salt bridge between R1229 and the acidic patch in nNOS means that once the contact is broken during domain−domain motion, wide separation such as that observed in the R1229E mutant is likely. The pre-steady-state reduction of cytochrome *c* by nNOSrd is a second-order process dependent on the collision frequency between cytochrome *c* and the FMN. The rate constants measured for CaM-bound wild-type nNOSrd, the R1229E mutant, and the isolated FMN domain are all very similar, indicating that the FMN is equally accessible in all three cases. This indicates that CaM binding induces a mainly open form of the enzyme, in which the FMN and FAD are not usually in contact. Electron transfer from FAD to FMN in the hinged closed form is likely to be very rapid over the 6 Å distance reported in the crystal structure, such that the hinged closed form may only need to be sampled briefly to maintain turnover.

Mutation of the acidic patch interface residues Glu816 and Glu762 (and R1229) has recently been shown to activate electron transfer through CaM-free nNOS and to slow the rate of electron transfer to nNOS heme (*38*). It has been speculated that the same residues interact with a basic patch on the oxygenase domain, including Lys423. Mutation of this residue has also been shown to affect the rate of NO synthesis (*39*). None of these mutations, or the R1229E mutant described here, result in the activation of NO synthesis in CaM-free nNOS. Thus, there is no direct correlation between the strength of interaction across the FMN−FAD domain interface and NO synthesis activity, although there is a relationship. It is interesting that the R1229E mutant, which appears to be forced into an open conformation, with little prospect of forming a stable flavin−flavin contact, is still affected by CaM binding in the steady-state cytochrome *c* reduction assays. CaM binding appears to enable the enzyme to open further, causing increased cytochrome *c*-dependent inhibition. Thus, in addition to releasing the "conformational lock" exhibited by nNOS reductase domain, CaM also appears to remove a "hinge stop", which prevents the two domains from swinging further apart. Such large-scale motion may be necessary for the FMN to deliver an electron to the heme. Various candidates for this structural feature are the autoinhibitory elements mentioned previously.

In summary, the R1229E mutation disrupts the FAD−FMN domain interface in nNOSrd such that there is no regulatory interaction between the two domains. Electron transfer from FAD to FMN is severely retarded, and hydride transfer from NADPH to FAD is accelerated, particularly when compared to the CaM-free wild-type enzyme. This is consistent with a model for the catalytic action of the enzyme in which it exists in two conformational states, "closed" and "open", with distinct kinetic events happening in each state (Figure 8). The "closed" form allows electron transfer from FAD to FMN, while the enzyme must be in the "open" form for both facile hydride transfer from NADPH to FAD and electron transfer from FMN to cytochrome *c* or nNOS heme. The presence of the salt bridge at Arg1229 is clearly essential for the successful movement of the FMN binding domain from an electron-receiving position to an electron-donating one and can be thought of as another regulatory feature in the complex structural makeup of nNOS.

REFERENCES

1. Schmidt, H., and Walter, U. (1994) NO at Work. *Cell 78*, 919–925.
2. Masters, B. S. S. (2000) in *Nitric Oxide, Biology and Pathobiology* (Ignarro L. J., Ed.) pp 91−104, Academic Press, New York.
3. Alderton, W. K., Cooper, C. E., and Knowles, R. G. (2001) Nitric oxide synthases: structure, function and inhibition. *Biochem. J. 357*, 593–615.
4. Stuehr, D. J. (1999) Mammalian nitric oxide synthases. *Biochim. Biophys. Acta 1411*, 217–230.
5. Siddhanta, U., Presta, A., Fan, B. C., Wolan, D., Rosseau, D. L., and Stuehr, D. J. (1998) Domain swapping in inducible nitric oxide synthase−Electron transfer occurs mainly between flavin and heme groups located on adjacent subunits in the dimer. *J. Biol. Chem. 273*, 18950–18958.
6. Sagami, I., Daff, S., and Shimizu, T. (2001) Intrasubunit and intersubunit electron transfer in neuronal nitric-oxide synthase: Effect of calmodulin on heterodimer catalysis. *J. Biol. Chem. 276*, 30036–30042.
7. Crane, B. R., Arvai, A. S., Ghosh, D. K., Wu, C., Getzoff, E. D., Stuehr, D. J., and Tainer, J. A. (1998) Structure of nitric oxide synthase oxygenase dimer with pterin and substrate. *Science 279*, 2121–2126.

8. Raman, C. S., Li, H., Martasek, P., Kral, V., Masters, B. S. S., and Poulos, T. L. (1998) Crystal structure of constitutive endothelial nitric oxide synthase: A Paradigm for pterin function involving a novel metal center. *Cell 95*, 939–950.
9. Stuehr, D. J., Santolini, J., Wang, Z., Wei, C., and Adak, S. (2004) Update on mechanism and catalytic regulation in the NO synthases. *J. Biol. Chem. 279*, 36167–36170.
10. Wang, M., Roberts, D. L., Paschke, R., Shea, T. M., Masters, B. S. S., and Kim, J. P. (1997) Three-dimensional structure of NADPH-cytochrome P450 reductase: prototype for FMN- and FAD-containing enzymes. *Proc. Natl. Acad. Sci. U.S.A. 94*, 8411–8416.
11. Garcin, E. D., Bruns, C. M., Lloyd, S. J., Hosfield, D. J., Tiso, M., Gacchui, R., Stuehr, D. J., Tainer, J. A., and Getzoff, E. D. (2004) Structural basis for isozyme-specific regulation of electron transfer in nitric oxide synthase. *J. Biol. Chem. 279*, 37918–37927.
12. Zhang, J., Martasek, P., Paschke, R., Shea, T., Masters, B. S. S., and Kim, J. P. (2001) Crystal structure of the FAD/NADPH-binding domains of rat neuronal nitric oxide synthase. *J. Biol. Chem. 276*, 37506–37513.
13. Masters, B. S. S. (1994) Nitric oxide synthase—why so complex. *Anuu. Rev. Nutr. 14*, 131–145.
14. Abu-Soud, H. M., and Stuehr, D. J. (1993) Nitric-oxide synthases reveal a role for calmodulin in controlling electron transfer. *Proc. Natl. Acad. Sci. U.S.A. 90*, 10769–10772.
15. Sagami, I., Sato, Y., Noguchi, T., Miyajima, M., Rozhkova, E., Daff, S., and Shimizu, T. (2002) Electron transfer in nitric-oxide synthase. *Coord. Chem. Rev. 226*, 179–186.
16. Gacchui, R., Presta, A., Bentley, D. F., Abu-Soud, H. M., McArthur, R., Brudvig, G., Ghosh, D. K., and Stuehr, D. J. (1996) Characterisation of the reductase domain of rat neuronal nitric oxide synthase generated in the methylotrophic yeast *Pichia pastoris*. *J. Biol. Chem. 271*, 20594–20602.
17. Noble, M. A., Munro, A. W., Rivers, S. L., Robledo, L., Daff, S. N., Yellowlees, L. J., Shimizu, T., Sagami, I., Guillemette, J. G., and Chapman, S. K. (1999) Potentiometric analysis of the flavin cofactors of neuronal nitric oxide synthase. *Biochemistry 38*, 16413–16418.
18. Guan, Z.-W., and Iyanagi, T. (2003) Electron transfer is activated by calmodulin in the flavin domain of human neuronal nitric oxide synthase. *Arch. Biochem. Biophys. 412*, 65–76.
19. Daff, S. (2003) Calmodulin-dependent regulaton of mammalian nitric oxide synthase. *Biochem. Soc. Trans. 31*, 502–505.
20. Salerno, J. C., Harris, D. E., Irizarry, K., Patel, B., Morales, A. J., Smith, S. M. E., Martasek, P., Roman, L. J., Masters, B. S. S., Jones, C. L., Weismann, B. A., Lane, P., Liu, Q., and Gross, S. S. (1997) An autoinhibitory control element defines calcium-regulated isoforms of nitric oxide synthase. *J. Biol. Chem. 272*, 29769–29777.
21. Daff, S., Sagami, I., and Shimizu, T. (1999) The 42-amino acid insert in the FMN domain of neuronal nitric oxide synthase exerts control over Ca^{2+}/calmodulin electron transfer. *J. Biol. Chem. 274*, 30589–30595.
22. Roman, L. J., Martasek, P., Miller, R. T., Harris, D. E., de la Garza, M. A., Shea, T. M., Kim, J.-J. P., and Masters, B. S. S. (2000) The C termini of constitutive nitric oxide synthases control electron flow through the flavin and heme domains and affect modulation by calmodulin. *J. Biol. Chem. 275*, 29225–29232.
23. Jachymova, M., Martasek, P., Panda, S., Roman, L. J., Panda, M., Shea, T. M., Ishimura, Y., Kim, J.-J. P., and Masters, B. S. S. (2005) Recruitment of governing elements for electron transfer in the nitric oxide synthase family. *Proc. Natl. Acad. Sci. U.S.A. 102*, 15833–15838.
24. Roman, L. J., Martasek, P., and Masters, B. S. S. (2002) Intrinsic and extrinsic modulation of nitric oxide synthase activity. *Chem. Rev. 102*, 1179–1189.
25. Roman, L. J., and Masters, B. S. S. (2006) Electron transfer by neuronal nitric oxide synthase is regulated by concerted interaction of calmodulin and two intrinsic regulatory elements. *J. Biol. Chem. 281*, 23111–23118.
26. Jones, R. J., Smith, S. M. E., Gao, Y. T., DeMay, B. S., Mann, K. J., Salerno, K. M., and Salerno, J. C. (2004) The function of the small insertion in the hinge subdomain in the control of constitutive mammalian nitric-oxide synthases. *J. Biol. Chem. 279*, 36876–36883.
27. Fulton, D., Gratton, J.-P., McCabe, T. J., Fontana, J., Fujio, Y., Walsh, K., Franke, T. F., Papapetropoulos, A., and Sessa, W. C. (1999) Regulation of endothelium-derived nitric oxide production by the protein kinase Akt. *Nature 399*, 597–601.
28. Adak, S., Santonlini, J., Tikunova, S., Wang, Q., Johnson, J. D., and Stuehr, D. J. (2001) Neuronal nitric oxide synthase mutant (Ser1412-Asp) demonstrates surprising connections between heme reduction, NO complex formation, and catalysis. *J. Biol. Chem. 276*, 1244–1252.
29. Tiso, M., Konas, D. W., Panda, K., Garcin, E. D., Sharma, M., Getzoff, E. D., and Stuehr, D. J. (2005) C-terminal residue Arg1400 enables NADPH to regulate electron transfer in neuronal nitric oxide synthase. *J. Biol. Chem. 280*, 39208–39219.
30. Adak, S., Sharma, M., Meade, A. L., and Stuehr, D. J. (2002) A conserved flavin-shielding residue regulates NO synthase electron transfer and nicotinamide coenzyme specificity. *Proc. Natl. Acad. Sci. U.S.A. 99*, 13516–13521.
31. Konas, D. W., Zhu, K., Sharma, M., Adak, K. S., Brudvig, G. W., and Stuehr, D. J. (2004) The FAD-shielding residue Phe1395 regulates neuronal nitric-oxide synthase catalysis by controlling $NADP^+$ affinity and a conformational equilibrium within the flavoprotein domain. *J. Biol. Chem. 279*, 35412–35425.
32. Craig, D. H., Chapman, S. K., and Daff, S. (2002) Calmodulin activates electron transfer through neuronal nitric oxide synthase reductase domain by releasing an NAPDH-dependent conformational lock. *J. Biol. Chem. 277*, 33987–33994.
33. Roman, L. J., Sheta, E. A., Martasek, P., Gross, S. S., Lui, Q., and Masters, B. S. S. (1995) High-level expression of functional rat neuronal nitric oxide synthase in *Escherichia coli*. *Proc. Natl. Acad. Sci. U.S.A. 92*, 8428–8432.
34. Newton, D. C., Montgomery, H. J., and Guillemette, J. G. (1998) The reductase domain of the human inducible nitric oxide synthase is fully active in the absence of bound calmodulin. *Arch. Biochem. Biophys. 359*, 249–257.
35. Goloubinoff, P., Gatenby, A. A., and Lorimer, G. H. (1989) GroE heat-shock proteins promote assembly of foreign prokaryotic ribulose bisphosphate carboxylase oligomers in *Eschericha coli*. *Nature 337*, 44–47.
36. Garnaud, P. E., Koetsier, M., Ost, T. W. B., and Daff, S. (2004) Redox properties of the isolated flavin mononucleotide- and flavin adenine dinucleotide-binding domains of neuronal nitric oxide synthase. *Biochemistry 43*, 11035–11044.
37. Dunford, A. J., Rigby, S. E. J., Hay, S., Munro, A. W., and Scrutton, N. S. (2007) Conformational and thermodynamic control of electron transfer in neuronal nitric oxide synthase. *Biochemistry 46*, 5018–5029.
38. Panda, K., Hague, M. M., Garcin-Hosfield, E. D., Durra, D., Getzoff, E. D., and Stuehr, D. J. (2006) Surface charge interactions of the FMN module govern catalysis by nitric-oxide synthase. *J. Biol. Chem. 281*, 36819–36827.
39. Shimanuki, T., Sato, H., Daff, S., Sagami, I., and Shimizu, T. (1999) Crucial role of Lys423 in the electron transfer of neuronal nitric oxide synthase. *J. Biol. Chem. 274*, 26956–26961.
40. Shen, A. L., and Kasper, C. B. (1995) Role of acidic residues in the interaction of NADPH-cytochrome P450 oxidoreductase and cytochrome *c*. *J. Biol. Chem. 270*, 27475–27480.
41. Feng, C., Tollin, G., Holliday, M. A., Thomas, C., Salerno, J. C., Enemark, J. H., and Ghosh, D. K. (2006) Intraprotein electron transfer in a two-domain construct of neuronal nitric oxide synthase: the output state in nitric oxide formation. *Biochemistry 45*, 6354–6362.
42. Ghosh, D. K., Holliday, M. A., Thomas, C., Weinberg, J. B., Smith, S. M. E., and Salerno, J. C. (2006) NOS output state; design and properties of nitric-oxide synthase oxygenase/FMN domain constructs. *J. Biol. Chem. 281*, 14173–14183.
43. Guan, Z.-W., Kamatani, D., Kimura, S., and Iyanagi, T. (2003) Mechanistic studies on the intramolecular one-electron transfer between the two flavins in the human neuronal nitric-oxide synthase and inducible nitric-oxide synthase flavin domains. *J. Biol. Chem. 278*, 30859–30868.
44. Knight, K., and Scrutton, N. S. (2002) Stopped-flow kinetic studies of electron transfer in the reductase domain of neuronal nitric oxide synthase: re-evaluation of the kinetic mechanism reveals new enzyme intermediates and variation with cytochrome P450 reductase. *Biochem. J. 367*, 19–30.

BI800787M